Cell Reports, Volume *41*

Supplemental information

Cms1 coordinates stepwise local 90S pre-ribosome assembly with timely snR83 release

Benjamin Lau, Olga Beine-Golovchuk, Markus Kornprobst, Jingdong Cheng, Dieter Kressler, Beáta Jády, Tamás Kiss, Roland Beckmann, and Ed Hurt

SUPPLEMENTAL INFORMATION

Cms1 coordinates stepwise local 90S pre-ribosome assembly with timely snR83 release

Benjamin Lau, Olga Beine-Golovchuk, Markus Kornprobst, Jingdong Cheng, Dieter Kressler, Beáta Jády, Tamás Kiss, Roland Beckmann and Ed Hurt

Supplementary Figures

Figure S1 – Figure S7P

Figure S1

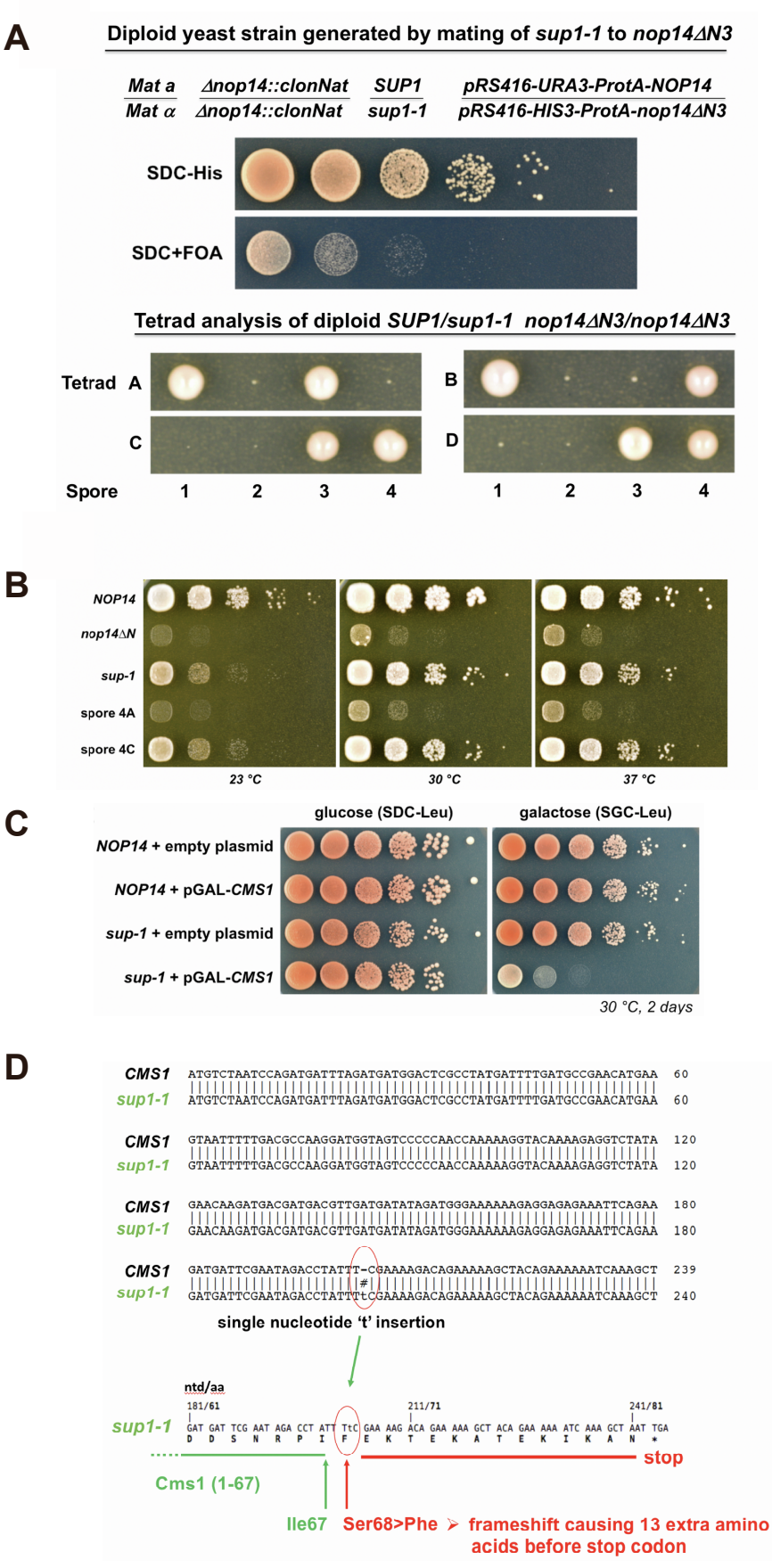
A
Diploid yeast strain generated by mating of sup1-1 to nop14ΔN3
Mat a / Mat α
Δnop14::clonNat / Δnop14::clonNat
SUP1 / sup1-1
pRS416-URA3-ProtA-NOP14 / pRS416-HIS3-ProtA-nop14ΔN3
SDC-His
SDC+FOA
Tetrad analysis of diploid SUP1/sup1-1 nop14ΔN3/nop14ΔN3
Tetrad A
B
C
D
Spore 1 2 3 4 1 2 3 4
B
NOP14
nop14ΔN
sup-1
spore 4A
spore 4C
23 °C
30 °C
37 °C
C
glucose (SDC-Leu)
galactose (SGC-Leu)
NOP14 + empty plasmid
NOP14 + pGAL-CMS1
sup-1 + empty plasmid
sup-1 + pGAL-CMS1
30 °C, 2 days
D
CMS1 ATGTCTAATCCAGATGATTTAGATGATGGACTCGCCTATGATTTTGATGCCGAACATGAA 60
sup1-1 ATGTCTAATCCAGATGATTTAGATGATGGACTCGCCTATGATTTTGATGCCGAACATGAA 60
CMS1 GTAATTTTTGACGCCAAGGATGGTAGTCCCCCAACCAAAAAGGTACAAAAGAGGTCTATA 120
sup1-1 GTAATTTTTGACGCCAAGGATGGTAGTCCCCCAACCAAAAAGGTACAAAAGAGGTCTATA 120
CMS1 GAACAAGATGACGATGACGTTGATGATATAGATGGGAAAAAAGAGGAGAGAAATTCAGAA 180
sup1-1 GAACAAGATGACGATGACGTTGATGATATAGATGGGAAAAAAGAGGAGAGAAATTCAGAA 180
CMS1 GATGATTCGAATAGACCTATTT-CGAAAAGACAGAAAAAGCTACAGAAAAAATCAAAGCT 239
sup1-1 GATGATTCGAATAGACCTATTTtCGAAAAGACAGAAAAAGCTACAGAAAAAATCAAAGCT 240
single nucleotide 't' insertion
ntd/aa
181/61 211/71 241/81
sup1-1 GAT GAT TCG AAT AGA CCT ATT TtC GAA AAG ACA GAA AAA GCT ACA GAA AAA ATC AAA GCT AAT TGA
D D S N R P I F E K T E K A T E K I K A N *
stop
Cms1 (1-67)
Ile67
Ser68>Phe ➢ frameshift causing 13 extra amino acids before stop codon

Figure S1. Genetic analysis of the *sup1-1* suppressor *derived from the nop14ΔN3* strain. Related to Figures 1 and 2.

(A) Mating of the *sup1-1* suppressor derived from the *nop14ΔN3* mutant to a *NOP14* shuffle strain (*Δnop14::clonNat*, pRS416-*URA3*-ProtA-*NOP14*) containing the pRS413-*HIS3*-ProtA-*nop14ΔN3* plasmid. When streaked on SDC+5-FOA, the derived diploid strain regained a slow-growing phenotype (upper panel), suggesting that the *sup1-1* mutation is recessive. This diploid strain was sporulated and tetrads were dissected, which revealed a 2:2 segregation of fast- and slow-growing colonies; all tetrad spores were HIS^+ indicating the presence of pRS413-*HIS3*-ProtA-*nop14ΔN3* plasmid (lower panel). Thus, two of the four tetrad spores revealed typical *sup1-1* suppressor activity, whereas the other two spores exhibit the slow-growing phenotype of the original *nop14ΔN3* mutant.

(B) Dot-spot growth analysis of the *sup1-1* suppressor strain derived from the *nop14ΔN3* mutant, as well as haploid progeny spore 4A and spore 4 (see panel A) after tetrad analysis.

(C) Plasmid-based *GAL-CMS1* expression in the *sup1-1* strain leads to loss of suppression. Wild-type cells and the *sup1-1* strain were transformed with empty or *GAL-CMS1* carrying *LEU2* plasmids, before representative transformants were grown on either glucose-containing (SDC−Leu) or galactose-containing (SGC−Leu) plates at 30°C for 2 days.

(D) The chromosomal mutation in the *sup1-1* suppressor strain is identified as a "T" insertion frameshift mutation within the *CMS1* gene. Genome sequencing of the *sup1-1* yeast strain (*nop14ΔN3* derived) identified a "T" nucleotide insertion in the nonessential *CMS1* gene leading to a drastically shortened protein. Upper panel: A cut out of the DNA sequence obtained from genomic sequencing, starting at the start codon of the *CMS1* gene from W303 wild-type yeast (*CMS1*) and the *sup1-1* suppressor strain and including the discovered "T" (t) insertion at position 202 in the *sup1-1* DNA sequence. Lower panel: By prediction, the T insertion mutation generates a truncated Cms1 protein (wild-type protein, 291 amino acids) with Ser68Phe at the insertion site, followed by a frameshifted 13-amino-acid long extension before a stop codon.

Figure S2

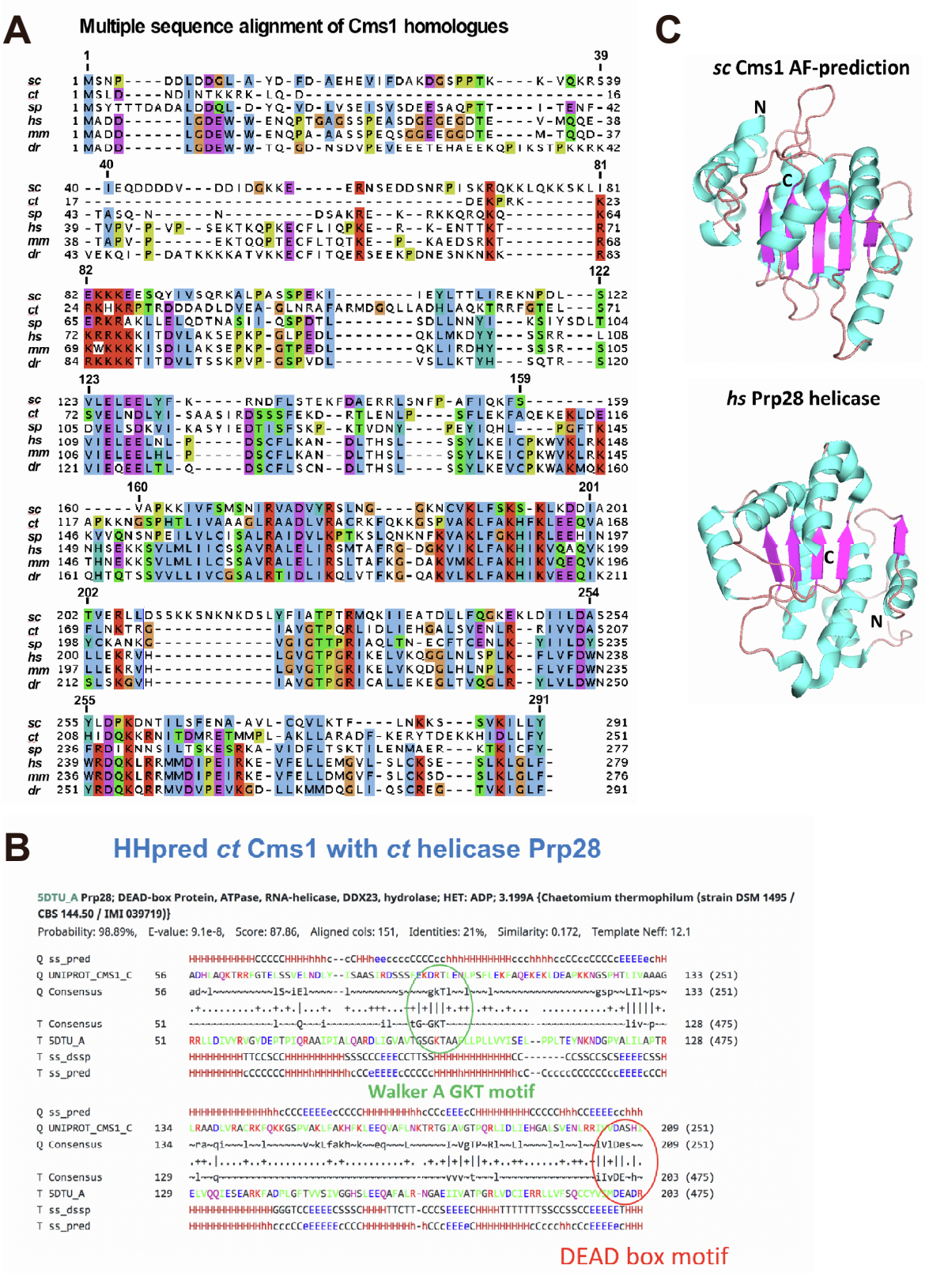
A
Multiple sequence alignment of Cms1 homologues
sc
ct
sp
hs
mm
dr
B
HHpred ct Cms1 with ct helicase Prp28
5DTU_A Prp28; DEAD-box Protein, ATPase, RNA-helicase, DDX23, hydrolase; HET: ADP; 3.199A {Chaetomium thermophilum (strain DSM 1495 / CBS 144.50 / IMI 039719)}
Probability: 98.89%, E-value: 9.1e-8, Score: 87.86, Aligned cols: 151, Identities: 21%, Similarity: 0.172, Template Neff: 12.1
Walker A GKT motif
DEAD box motif
C
sc Cms1 AF-prediction
N
C
hs Prp28 helicase
C
N

Figure S2. The conserved Cms1 has a helicase fold but lacks typical helicase motifs. Related to Figures 1 and 2.

(A) Multiple sequence alignment of Cms1 homologues from *Saccharomyces cerevisiae* (*sc*), *Chaetomium thermophilum* (*ct*), *Schizosaccharomyces pombe* (*sp), Homo sapiens* (*hs*), *Mus musculus* (*mm*) and *Danio rerio* (*dr*). Cms1 has a predicted helicase fold but lacks functional motifs (e.g. Walker A, DEAD box) and consists of only one of the two RecA-like helicase domains.

(B) Secondary structure prediction (https://toolkit.tuebingen.mpg.de/hhpred) of *ct*Cms1 in comparison to crystallized *ct*Prp28 helicase. Note that Cms1 lacks typical helicase motifs such as Walker A (ATP binding) and DEAD box.

(C) Alpha-fold prediction (https://alphafold.ebi.ac.uk/entry/P12270) of yeast Cms1 in comparison to the crystal structure of a classical helicase (*hs* Prp28, PDB: 4NHO; only the first helicase RecA-like domain is shown). Only the part of the structures (*sc*Cms1 residues 94–289; *hs*Prp28 residues 391–569) exhibiting structural homology is shown.

Figure S3

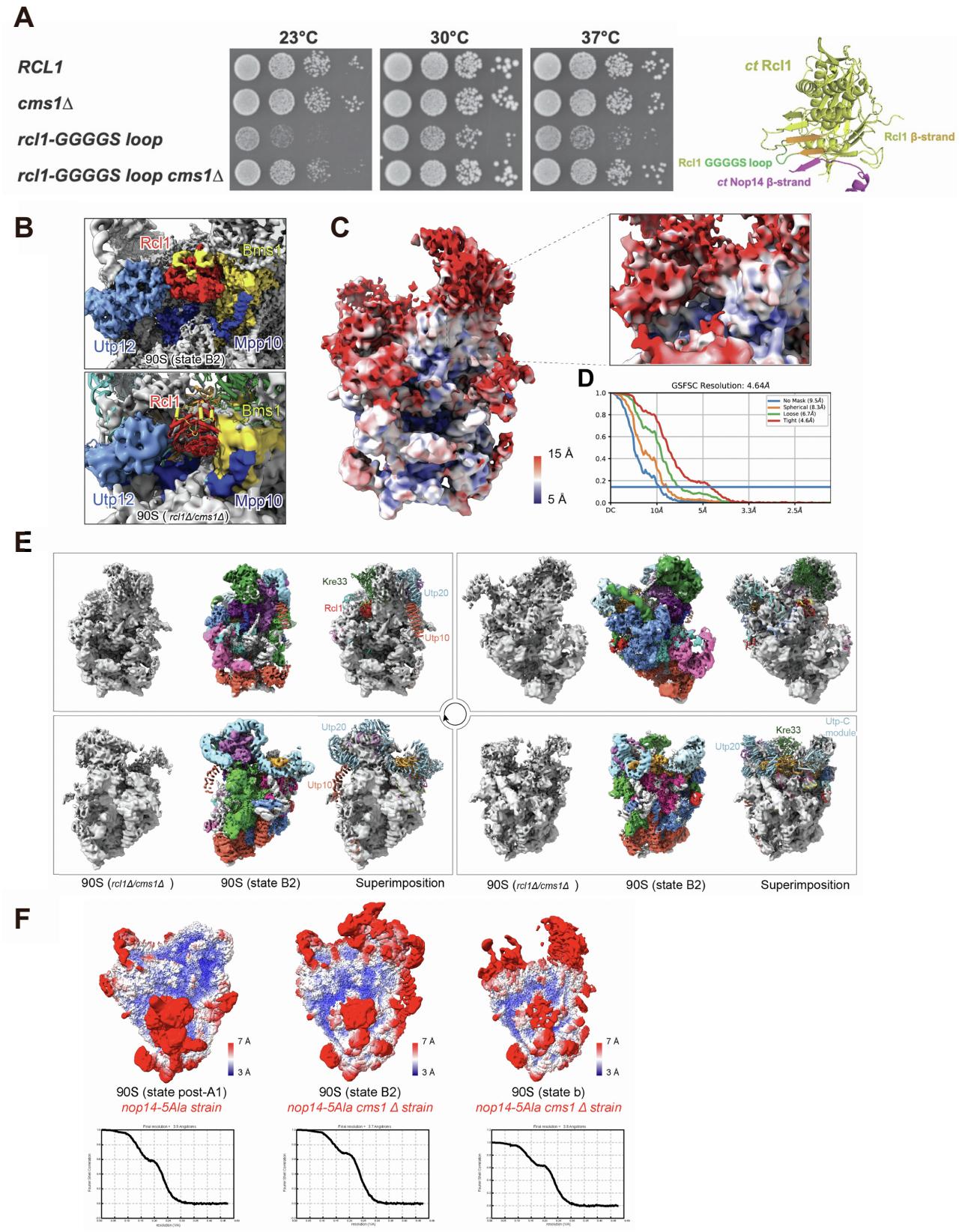
A
23°C
30°C
37°C
RCL1
cms1Δ
rcl1-GGGGS loop
rcl1-GGGGS loop cms1Δ
ct Rcl1
Rcl1 β-strand
Rcl1 GGGGS loop
ct Nop14 β-strand
B
Rcl1
Bms1
Utp12
Mpp10
90S (state B2)
90S (rcl1Δ/cms1Δ)
C
15 Å
5 Å
D
GSFSC Resolution: 4.64Å
No Mask (9.5Å)
Spherical (8.3Å)
Loose (6.7Å)
Tight (4.6Å)
E
Kre33
Utp20
Rcl1
Utp10
Utp-C module
90S (rcl1Δ/cms1Δ)
90S (state B2)
Superimposition
F
7 Å
3 Å
90S (state post-A1)
nop14-5Ala strain
90S (state B2)
nop14-5Ala cms1 Δ strain
90S (state b)
nop14-5Ala cms1 Δ strain

Figure S3. Different *rcl1* mutants and the *nop14-5Ala* strain are suppressed by *cms1Δ.* Related to Figures 2 and 3.

(A) Slow-growth phenotype of the *rcl1-GGGS loop* mutant suppressed by *cms1Δ.* Left part: Dot-spot growth analysis of wild-type *RCL1* yeast (W303), single *cms1Δ* and *rcl1-GGGGS loop* mutants, and double-mutant *rcl1-GGGGS loop cms1Δ*. Cells were grown at 23°C, 30°C, and 37°C for 2 days. Right part: Rcl1 structure (yellow), extracted from the *Chaetomium thermophilum ct*Noc4–Kre33 90S pre-ribosome (PDB: 6RXU, 6RXV), is built from several β-strands, of which a peripheral strand (orange) aligns with a β-strand in the Nop14 N terminus (magenta). From that β-strand emerges a loop connecting another adjacent Rcl1 β-strand (orange); this loop has been replaced by a glycine–serine (GGGGS) linker (green; predicted length 19 Å), resulting in the *rcl1-GGGGS loop* mutant

(B-E) Cryo-EM analysis of 90S pre-ribosomal particles, isolated from the double-disruption *rcl1Δ cms1Δ* strain via the 90S bait protein FTpA-Utp18. For comparison, the cryo-EM structure of an intact yeast 90S particle in state B2 (EMD-11358) is shown.

(B) Depicted for comparison are the cryo-EM structures focusing on the Rcl1 region of an intact yeast 90S (state B2) (EMD-11358, up) and of the 90S from the double-disruption *rcl1Δ cms1Δ* strain (down). Superimposition of the molecular model of the 90S (state B2) (PDB:6ZQB) with the 90S (*rcl1Δ cms1Δ*) density map was shown to illustrate the difference.

(C) Local resolution distribution of the 90S particle (*rcl1Δ cms1Δ*) calculated in Relion. A focusing view on the Rcl1 region is shown as an insert on the top-right.

(D) Gold-standard FSC curve of the 90S structure (*rcl1Δ cms1Δ*) calculated in cryoSPARC. The overall resolution of the 90S from the *rcl1Δ cms1Δ* strain is 6.7 Å (using a loose mask from cryoSPARC).

(E) Four different comparative views of the 90S (state B2 wild-type) and 90S (*rcl1Δ cms1Δ*). The 90S structures (*rcl1Δ cms1Δ*) are shown on the left, while the 90S (state B2) structures in a related orientation are shown in the middle. The superimposition of the 90S (*rcl1Δ cms1Δ*) with 90S (state B2 wild-type) molecular model are shown on the right.

(F) Local resolution distributions and FSC curves of different 90S particles isolated via Dhr1-Dim1 from mutants *nop14-5Ala* (left panel; see Figure 3C), and via FTpA-Utp18 from *nop14-5Ala cms1Δ* (middle and right panel; see Figure 2D).

Figure S4

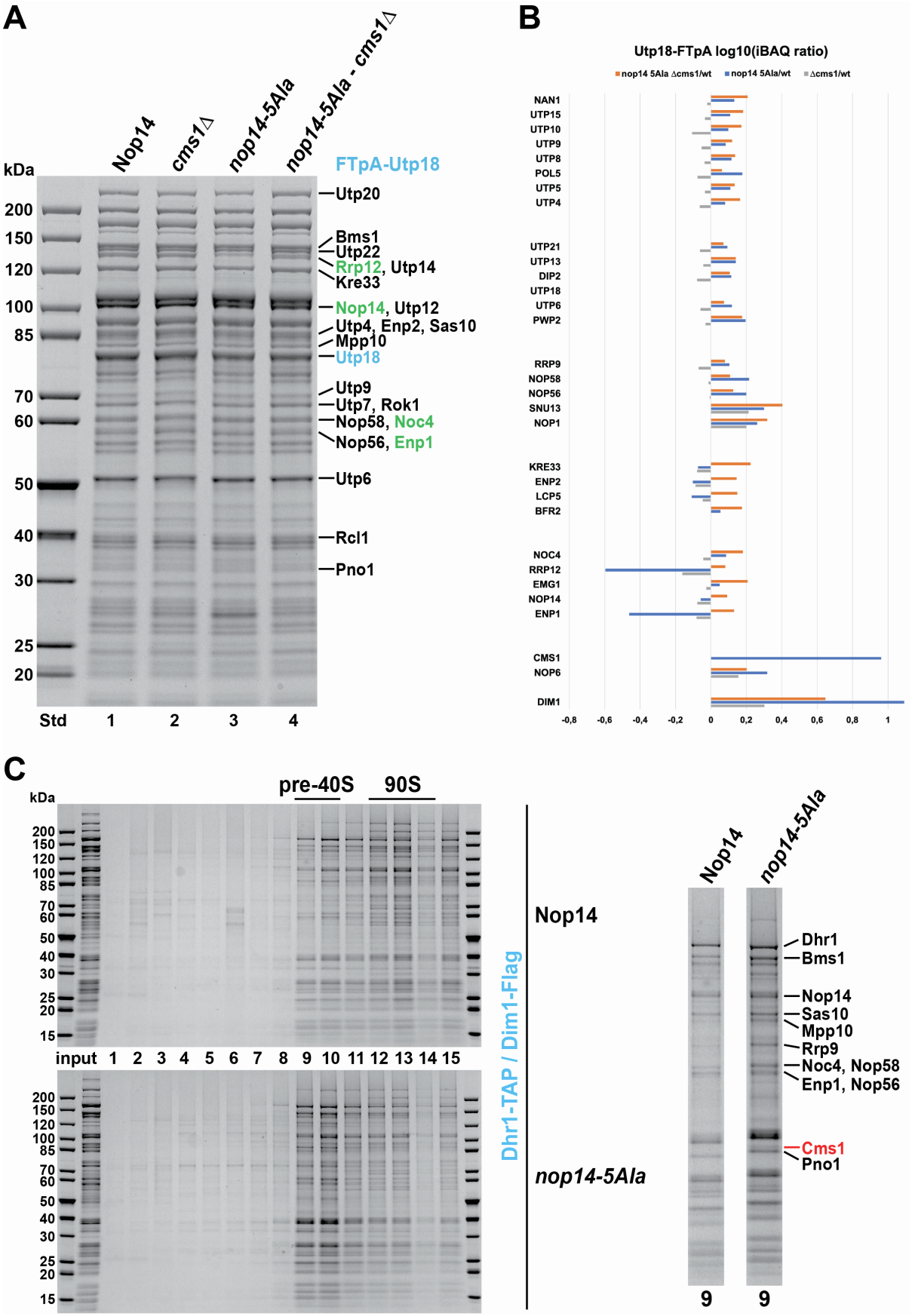
A
Nop14
cms1Δ
nop14-5Ala
nop14-5Ala - cms1Δ
kDa
FTpA-Utp18
200
150
120
100
85
70
60
50
40
30
25
20
Utp20
Bms1
Utp22
Rrp12, Utp14
Kre33
Nop14, Utp12
Utp4, Enp2, Sas10
Mpp10
Utp18
Utp9
Utp7, Rok1
Nop58, Noc4
Nop56, Enp1
Utp6
Rcl1
Pno1
Std 1 2 3 4
B
Utp18-FTpA log10(iBAQ ratio)
nop14 5Ala Δcms1/wt
nop14 5Ala/wt
Δcms1/wt
NAN1
UTP15
UTP10
UTP9
UTP8
POL5
UTP5
UTP4
UTP21
UTP13
DIP2
UTP18
UTP6
PWP2
RRP9
NOP58
NOP56
SNU13
NOP1
KRE33
ENP2
LCP5
BFR2
NOC4
RRP12
EMG1
NOP14
ENP1
CMS1
NOP6
DIM1
-0,8 -0,6 -0,4 -0,2 0 0,2 0,4 0,6 0,8 1
C
pre-40S
90S
kDa
200
150
120
100
85
70
60
50
40
30
25
20
15
input 1 2 3 4 5 6 7 8 9 10 11 12 13 14 15
Dhr1-TAP / Dim1-Flag
Nop14
nop14-5Ala
Nop14
nop14-5Ala
Dhr1
Bms1
Nop14
Sas10
Mpp10
Rrp9
Noc4, Nop58
Enp1, Nop56
Cms1
Pno1
9
9

Figure S4. Affinity purification of the different 90S particles from *nop14-5Ala* mutant and *nop14-5Ala cms1Δ* suppressor. Related to Figure 3.

(A, B) Utp18-FTpA was affinity purified in a second independent experiment, similar to that shown in Figure 3A, from wild-type yeast (*NOP14*), *cms1Δ* mutant, *nop14-5Ala* mutant, and *nop14-5Ala cms1Δ* suppressor. The final eluates were analyzed on a 4–12% gradient SDS-polyacrylamide gel with Coomassie Blue staining (A), or by semiquantitative mass spectrometry (B) as described in Method Details. The label-free quantification (intensity-based absolute quantification, iBAQ) values obtained for the co-enriched 90S factors were normalized to the Utp18 bait protein, which itself was set to 1. The iBAQ ratios of *cms1Δ* versus wild-type (wt) values (gray bars), *nop14-5AlaΔ* versus wt (blue bars), and *nop14-5Ala cms1Δ* versus wt (orange bars) are shown as $\log_{10}$-fold increase ("+" values on the x axis) or decrease ("−" values on the x axis). The whole set of iBAQ values from this semiquantitative mass spectrometry analysis is shown in Table S1.

(C) Sucrose gradient centrifugation of Dhr1–Dim1 split-tag affinity-purified 90S>pre-40S particles isolated from the wild type (*NOP14*, upper panel) and the *nop14-5Ala* mutant (lower panel). The final eluates were loaded onto a 15–45% sucrose gradient and the collected fractions 1–15 were analyzed on a 4–12% gradient SDS-polyacrylamide gel and stained with Coomassie Blue. Fractions 9 containing primordial pre-40S particles are separately displayed on the right, and the bands indicated were identified by mass spectrometry.

Figure S5

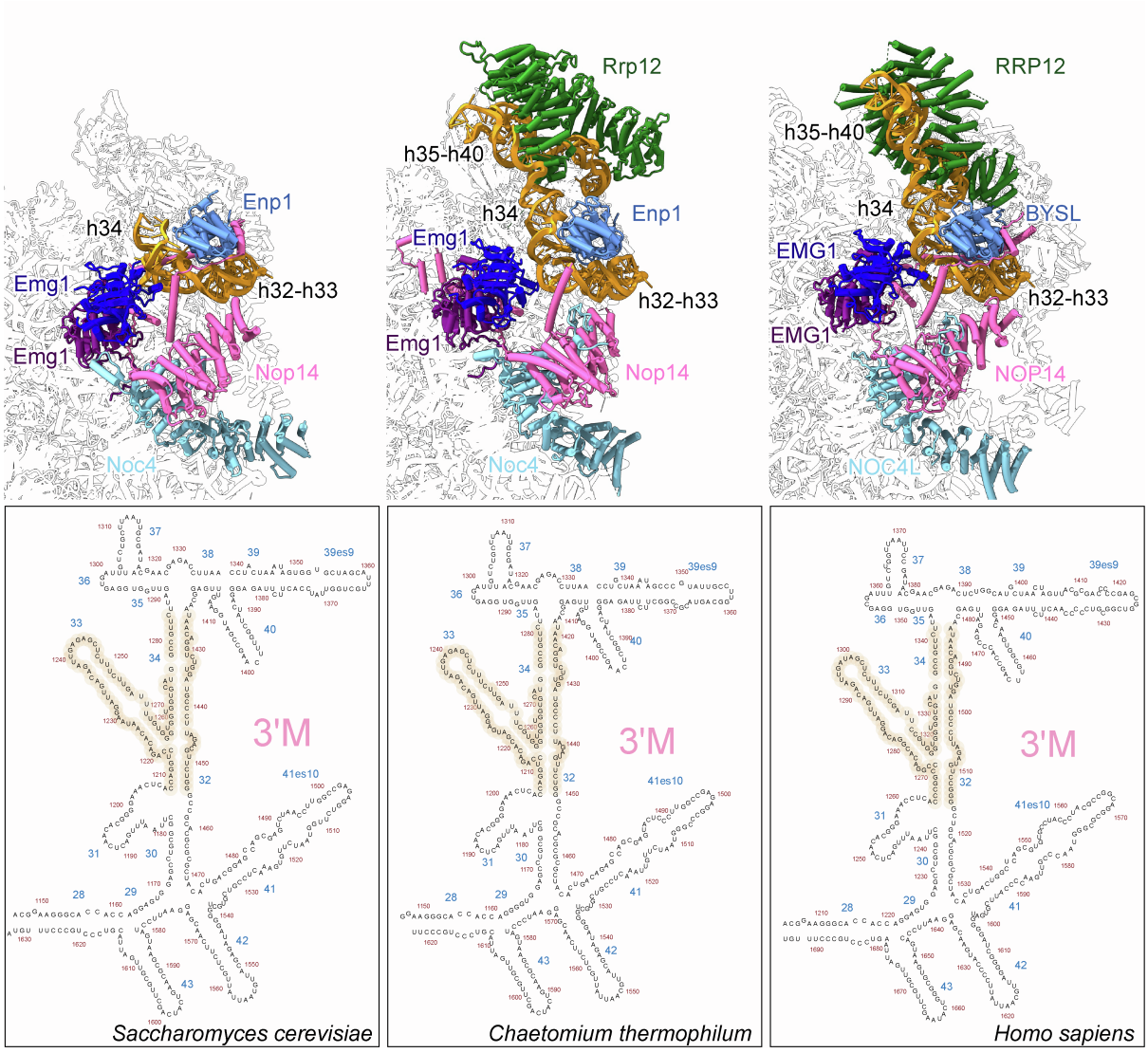

Figure S5. Conserved Noc4 module components Rrp12 and Enp1 establish a specific interaction with the 3'-major domain of the 18S rRNA. Related to Figures 2 and 4.

The cryo-EM structures of *Saccharomyces cerevisiae* (PDB: 6ZQC), *Chaetomium thermophilum* (PDB: 6RXU, updated), and *Homo sapiens* (PDB: 7MQA) 90S particles in the region of the Noc4–Nop14–Emg1–Enp1–Rrp12 module, which interacts with the 3' major domain. In human and *ct* 90S, BYSL/Enp1 is wedged between H32–H33–H34 and the RRP12 α-solenoid that encircles H35–H40.

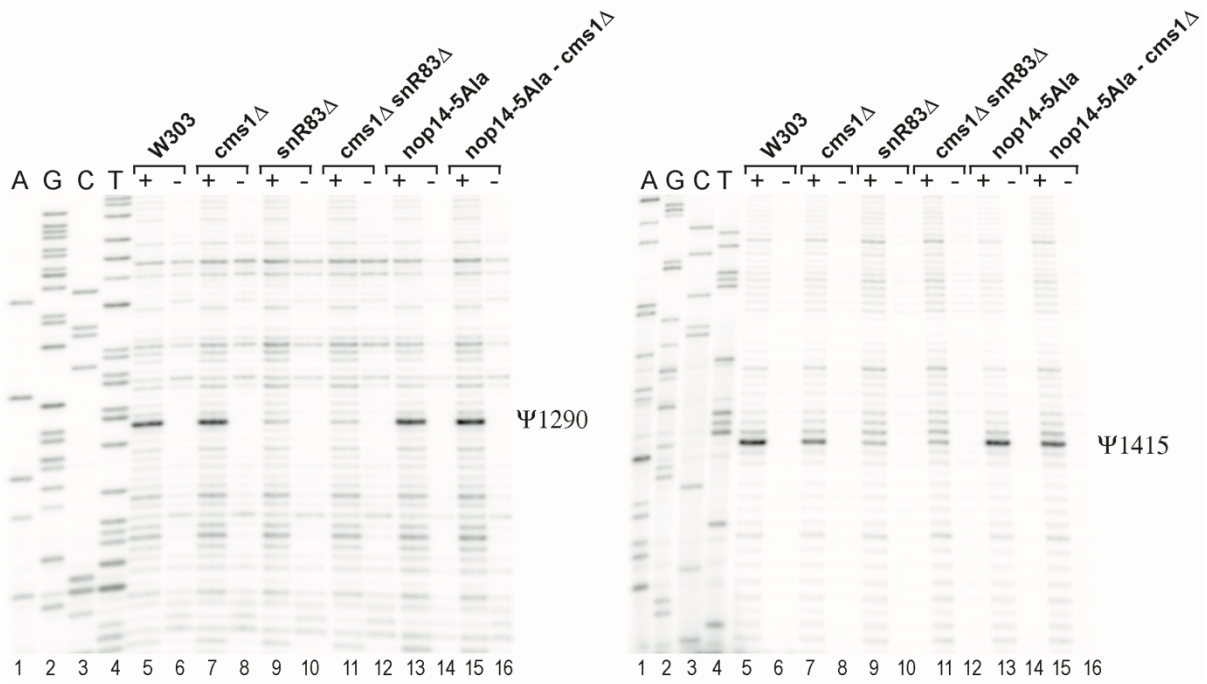

Figure S6. Pseudouridylation assay reveals that Cms1 is not required for snR83 guided Ψ 1290 and Ψ 1415 modifications in the yeast 18S rRNA. Related to Figure 5 and 6.

Pseudouridylation mapping of snR83 catalyzed modifications Ψ 1290 and Ψ 1415 in the 18S rRNA extracted from the indicated yeast strains. Ψs covalently modified by CMCT (N^3-1-cyclohexyl-3-(2-morpholinoethyl)carbodiimide metho-*p*-toluenesulfonate) were detected by primer extension analysis using terminally labeled 18S-specific primers and AMV reverse transcriptase. Lanes 1-4: A,G,C,T dideoxy sequencing reactions performed on 18S ribosomal DNA with the same 18S-specific primers. Lanes 5-16 : primer extension analysis using total RNA extracted from W303 (our wild-type yeast), *cms1Δ, snR83Δ, cms1Δ snR83Δ, nop14-5Ala and nop14-5Ala - cms1Δ* strains with (+) or without (-) previous CMCT-treatment. Ψ 1290 and Ψ 1415 are detected as RT stop signals and are indicated on the right. We noticed that the Ψ 1415, but not the Ψ 1290 modification was consistently decreased in the *cms1Δ* strains.

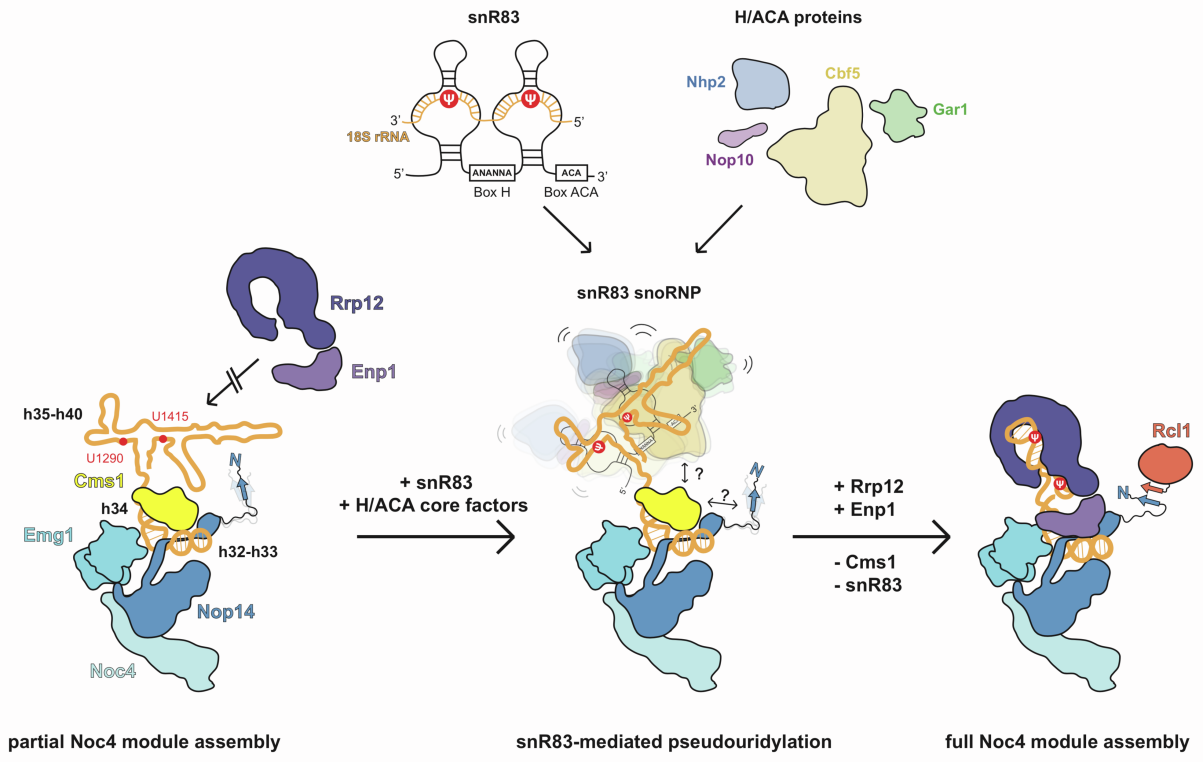

Figure S7. Model of Cms1 function at the 3'-major domain in coordination with stepwise Noc4 module assembly during early 90S biogenesis. Related to Figures 5-7.

Scheme of the stepwise Noc4 module assembly in the region of the 18S rRNA 3' major domain, consisting of rRNA helices h32-h40, within the 90S pre-ribosome. At an early phase (left), Noc4-Nop14-Emg1 members, but not Rrp12-Enp1, are bound to the 3'-major domain (partial Noc4 module assembly), at which also Cms1 is present by docking to h32-h34. This hinders Rrp12-Enp1 binding, but allows snR83 with its box H/ACA core factors (Cbf5, Gar1, Nhp2, Nop10) to bind to the exposed h35-h40 region to catalyze the pseudouridylation at two specific target sites, U1290 and U1415 (middle). Following this modification reaction, Cms1 and snR83 leave the 90S, allowing Rrp12-Enp1 to enter and complete Noc4 module assembly during 90S maturation (right). Finally, the Nop14 N-terminal β-blade contacts another β-blade in Rcl1, which could provide a signal for the next maturation steps until the 90S>pre-40S transition. For further explanations, see main text.